ELSEVIER

Colloids and Surfaces
A: Physicochemical and Engineering Aspects 143 (1998) 197–210

COLLOIDS AND SURFACES A

Contact angle measurements by axisymmetric drop shape analysis and an automated polynomial fit program☆

O.I. del Río, D.Y. Kwok, R. Wu, J.M. Alvarez, A.W. Neumann *

Department of Mechanical and Industrial Engineering, University of Toronto, 5 King's College Road, Toronto, Ontario, Canada, M5S 3G8

Received 20 January 1997; accepted 13 August 1997

Abstract

Low-rate dynamic contact angles of eight liquids on an inert (non-polar) FC-722 surface and a non-inert (polar) poly(propene-*alt*-*N*-methylmaleimide) copolymer are reported using two different contact angle methods: axisymmetric drop shape analysis (ADSA) and an automated polynomial fit (APF) scheme. The latter technique was found to be more sensitive to minute surface heterogeneity and/or roughness of the surface. For the non-inert solid–liquid systems, very complex contact angle responses were observed with both methods. If one omits these inconclusive contact angle measurements, the values of $\gamma_{lv} \cos \theta$ change smoothly with γ_{lv} for these polymers, independent of which of the two methods is used. When comparing with previously studied maleimide copolymer surfaces, a consistent change in the wettability was observed as the length of the side chains decreases from hexyl to methyl groups.

Keywords: Contact angle, drop shape; Contact angle, polynomial fit; Contact angle, dynamic; Surface tension, from contact angle; Surface tension, fluorocarbon

1. Introduction

It was shown elsewhere [1] that measuring contact angles at low rates of advance of the three-phase contact line by axisymmetric drop shape analysis–profile (ADSA-P) allows one to distinguish meaningful contact angles from meaningless ones on non-inert solid–liquid systems. Although the contact angles observed by ADSA-P and a goniometer were shown to be essentially identical for inert solid–liquid systems, it was found that contact angle measurements from the latter technique are liable to produce a mixture of meaningful and meaningless contact angles for non-inert systems, with no criteria to distinguish between the two. Thus, caution should be exercised when a goniometer/sessile drop technique is used for measuring contact angles. However, one might argue that the comparison in the previous paper between ADSA-P results and tangents to sessile drops (using a goniometer) might be misleading, in that the real difference between the two types of experiment was that between a fairly sophisticated and automated low-rate dynamic contact angle measurement and a very simple if not crude static measurement. To explore this thought we report here a novel, automated method called automated polynomial fit (APF) to put tangents to the same drop images on which ADSA-P operates. Thus,

* Corresponding author. Tel.: +1 416 9781270;
Fax: +1 416 9787753; e-mail: neumann@me.utovonto.ca

☆ This paper represents, in part, the PhD theses of D.Y. Kwok and O.I. del Río.

0927-7757/98/$ – see front matter
PII S0927-7757(98)00257-X

low-rate dynamic contact angle measurements are interpreted separately by two different schemes: ADSA-P and APF. Two types of solid surface were used: an inert FC-722-coated wafer surface and a non-inert (polar) poly(propene-*alt*-*N*-methylmaleimide) copolymer surface. For a comparison in terms of wettability, the latter copolymer surface was chosen, which is similar to those used in a previous paper [1] but with a different side chain.

2. Contact angle measurements

2.1. Axisymmetric drop shape analysis–profile (ADSA-P)

ADSA-P is a technique to determine liquid-fluid interfacial tensions and contact angles from the shape of axisymmetric menisci, i.e., from sessile as well as pendant drops. Assuming that the experimental drop is Laplacian and axisymmetric, ADSA-P finds the theoretical profile that best matches the drop profile extracted from the image of a real drop, from which the surface tension, contact angle, drop volume and surface area can be computed. The strategy employed is to fit the shape of an experimental drop to a theoretical drop profile according to the Laplace equation of capillarity, by using the surface/interfacial tension as an adjustable parameter. The best fit identifies the correct surface/interfacial tension and contact angle. Details of the methodology and experimental set-up can be found elsewhere [2–5].

2.2. Automated polynomial fit (APF)

Preliminary tests have shown that the use of straight lines or low-order polynomials (e.g., quadratic or cubic) to fit a few profile points near the contact line can produce large contact angle errors and is too sensitive to noise and to the number of points used. For the automated polynomial fit (APF) program described here, a high-order polynomial scheme with a variable number of points was implemented. The procedure is as follows.

The drop profile coordinates are extracted from a digital image with sub-pixel resolution with the same image-analysis techniques employed with ADSA-P: i.e., a Sobel gradient operator with cubic-splines interpolation [3,4], which generates several hundred pixel coordinates for each image.

A high-order polynomial of the form

$$z=\sum_{i=0}^{M} a_i x_i \tag{1}$$

where M is the order of the polynomial, is then fitted to the first $N=20$ points at the three-phase contact line on one side of the drop by using a least-squares algorithm, and the correlation coefficient R^2 is computed; N is increased and the procedure is repeated until approximately half of the profile has been used. The contact angle is then computed from the first derivative of the polynomial fit with the highest correlation coefficient, as

$$\theta=\tan^{-1}\left(\frac{\mathrm{d}z}{\mathrm{d}x}\right)$$

The same algorithm is then applied to the other side of the profile, producing a second contact angle, which might be slightly different from the first one if the drop is not perfectly axisymmetric or if there is noise in the data points close to the contact points. In the ideal case of perfectly axisymmetric and noiseless profile coordinates, such as numerically generated drop profiles (see below), the contact angles on both sides of the drop would be exactly the same. On real drops, however, the contact angles on both sides of the drops will, in general, be slightly different.

In some cases, particularly for contact angles close to 180°, it was found that a polynomial of the form

$$x=\sum_{i=0}^{M} a_i z_i \tag{2}$$

which is equivalent to a 90° rotation of the drop, might yield a better fit. The above procedure is then repeated by using the polynomial form (2), producing two additional contact angles (one for each side of the drop).

To estimate the actual contact angle for each drop, the four results computed by the program can, in principle, be averaged. However, the results obtained with either polynomial form can differ

significantly from the ones obtained using the other form, or the contact angle obtained by fitting one half of the profile can be significantly different from the one obtained using the other half due to noise in the profile coordinates near the contact line. In the case of only a few drop profiles, the results can be compared visually with the drop profile by plotting the polynomial fits on top of the actual drop profile, and results from the polynomial fits that deviate significantly from the profile near the contact line or that present non-Laplacian inflection points (see later) can be rejected. However, for an automated procedure that can be applied to many drop images without user intervention, a more practical approach must be sought.

To study the behaviour of the algorithm, in order to determine the optimum polynomial order M that can be used, and to develop criteria to automate the procedure, the program was tested on both computer-generated Laplacian drop profiles as well as experimental drops. Use of numerically generated drop profiles has the advantage that the results of the APF program can be compared with known contact angle values, which gives a clear indication of the accuracy of the algorithm, while by using real images of experimental drops, the sensitivity of the algorithm to real, imperfect data (noise) can be measured.

Theoretical sessile drop profiles with different contact angles were generated by numerically integrating the Laplace equation of capillarity by using the ALFI program [6]. A capillary constant, $c=(\Delta\rho)g/\gamma$, of 13.45 cm^{-2} and apex curvature, b, of 0.734 cm^{-1}, which correspond to a water–air system, were used. Fig. 1 shows the profile corresponding to a contact angle of 180°. Table 1 shows

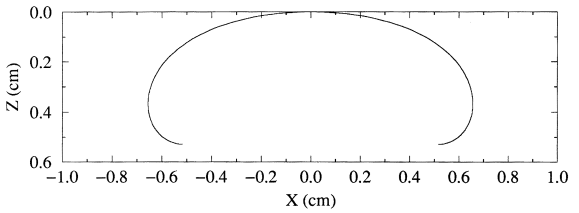

Fig. 1. Numerically generated sessile drop profile of a water–air system with contact angle of 180°, used to test the automated polynomial fit (APF) program.

the exact contact angles and the contact angle errors obtained with the APF algorithm by using different values of the polynomial order M. Since the theoretical drop profiles are perfectly symmetrical, the contact angles at both sides of the profile are identical and only one of them is shown (denoted as θ). In Table 1, $\theta_{1,err}$ and $\theta_{2,err}$ are the error (i.e., difference) between the real contact angle and the contact angle computed by using the polynomial forms (1) and (2), respectively. It can be seen that, for θ near 90°, polynomial form (2) gives larger errors and θ from form (1) is more accurate, while for θ near 180°, polynomial form (1) gives larger errors and θ from form (2) is more accurate. However, in all cases shown in Table 1, either polynomial form (1) or (2) gives very accurate results, and the contact angle error θ_{err} can be represented as the smaller of $\theta_{1,err}$ and $\theta_{2,err}$. Focusing on θ_{err} for different M shows that more accurate results can be obtained with the polynomial orders $M>5$. It should be noted that when ADSA-P was applied to these theoretical profiles, the exact contact angle was returned in all cases. Therefore, it is believed that the contact angles from ADSA-P are more accurate than those from the APF program.

To test the behaviour of the APF method with actual images of sessile drops, the program was applied to the image of the sessile drop shown in Fig. 2, in which the profile coordinates found by the image analysis software have been superimposed on the drop image. It should be noted that the extracted profile coordinates have sub-pixel resolution; however, the laser printer used to produce Fig. 2 has only pixel resolution and hence the coordinates shown in Fig. 2 can only reflect the resolution of the printer. Table 2 shows the contact angles obtained with both polynomial forms on both sides of the drop, using different polynomial order values M, and the contact angle obtained with ADSA-P. It can be seen that the higher the polynomial order the better the agreement between the contact angles computed by APF and ADSA-P. However, for this particular drop and in a similar fashion as with theoretical drops, one of the polynomial fits produces larger errors while the other one is more accurate when $M>5$. A closer view of the left-hand side of the drop at the

Table 1
Polynomial-fit contact angle errors for numerically generated drop profiles of water with different contact angles using different values of the polynomial order M. $\theta_{1,err}$ and $\theta_{2,err}$ are the contact angle errors obtained by using the polynomial forms (1) and (2) respectively; θ_{err} is the smaller of $\theta_{1,err}$ and $\theta_{2,err}$. All units are in degrees

	M	$\theta=5^\circ$	$\theta=30^\circ$	$\theta=60^\circ$	$\theta=90^\circ$	$\theta=120^\circ$	$\theta=150^\circ$	$\theta=180^\circ$
$\theta_{1,err}$	3	3.8×10^{-4}	0.021	0.025	0.048	0.247	1.32	8.26
$\theta_{2,err}$		6.0×10^{-6}	0.012	0.202	8.0	6.07	1.28	0.479
θ_{err}		6.0×10^{-6}	0.012	0.025	0.048	0.247	1.28	0.479
$\theta_{1,err}$	5	3.7×10^{-4}	3.2×10^{-5}	8.1×10^{-5}	2.9×10^{-4}	7.1×10^{-3}	0.156	5.96
$\theta_{2,err}$		3.1×10^{-5}	7.6×10^{-5}	7.6×10^{-5}	5.73	2.76	0.107	0.015
θ_{err}		3.1×10^{-5}	3.2×10^{-5}	8.1×10^{-5}	2.9×10^{-4}	7.1×10^{-3}	0.107	0.015
$\theta_{1,err}$	8	3.9×10^{-4}	2.1×10^{-4}	2.6×10^{-5}	1.9×10^{-5}	7.8×10^{-5}	5.5×10^{-3}	14.35
$\theta_{2,err}$		5.0×10^{-6}	5.8×10^{-5}	6.6×10^{-5}	3.60	0.27	3.4×10^{-3}	4.1×10^{-5}
θ_{err}		5.0×10^{-6}	5.8×10^{-5}	2.6×10^{-5}	1.9×10^{-5}	7.8×10^{-5}	3.4×10^{-3}	4.1×10^{-5}
$\theta_{1,err}$	10	3.8×10^{-4}	2.4×10^{-4}	1.3×10^{-4}	4.9×10^{-5}	3.7×10^{-5}	3.1×10^{-3}	11.84
$\theta_{2,err}$		4.0×10^{-6}	3.2×10^{-5}	1.7×10^{-4}	4.26	1.31	2.9×10^{-3}	3.4×10^{-4}
θ_{err}		4.0×10^{-6}	3.2×10^{-5}	1.3×10^{-4}	4.9×10^{-5}	3.7×10^{-5}	2.9×10^{-3}	3.4×10^{-4}

contact point (Fig. 3) reveals that the polynomial form (2) presents an inflection very close to the contact point because of noise in the profile points. Similarly, at the right-hand side (Fig. 4), polynomial form (2) overestimates the contact angle because of a noisy last coordinate point. Thus, the results from polynomial form (2) can be rejected in this case.

Since it appears that the higher the polynomial order M, the better the agreement between APF and ADSA, it would be tempting to use even larger values of M. However, it was found that for $M>10$ round-off numerical errors become important and the results start to deteriorate. Therefore, a polynomial order of $M=10$ is a better choice and was used in this study.

At this point, it is apparent that generating a satisfactory scheme such as APF for the purpose of contact angle measurement is not a trivial task, and commercially available schemes should be used with caution. If only a few images are to be processed, the above procedure may be usable. But for more advanced studies, such as large-scale dynamic contact angle studies to establish the thermodynamic significance of the experimental contact angles [7], this is impractical. For the

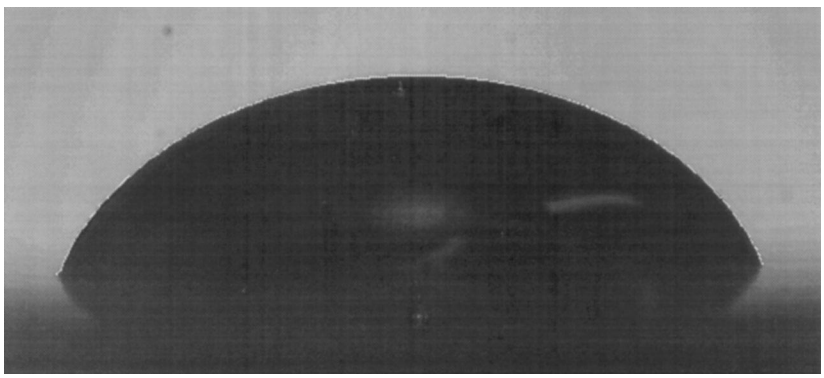

Fig. 2. Image of an experimental sessile drop used to test the APF program. The profile coordinates detected by the image analysis software have been superimposed on the image.

Table 2
Contact angle measurements for the sessile drop of Fig. 2 using the two forms of the polynomial fit and ADSA-P. R^2 is the correlation coefficient and N is the number of points that gave the best polynomial fit. Only one contact angle is computed by ADSA-P since it assumes an axisymmetric drop; the 95% confidence limit obtained by running ADSA-P 10 times with 20 different points is 0.23. The angles are in degrees

	M	Left			Right			Average
		θ_L	R^2	N	θ_R	R^2	N	θ_{AV}
θ_1	3	63.76	0.99955	116	62.42	0.99965	113	63.09
θ_2		64.27	0.99982	134	62.81	0.99984	128	63.54
θ_1	5	64.74	0.99988	215	63.32	0.99990	209	64.03
θ_2		62.45	0.99992	182	63.50	0.99993	176	62.97
θ_1	8	66.50	0.99994	311	65.10	0.99996	302	65.80
θ_2		58.75	0.99995	215	82.69	0.99996	209	—
θ_1	10	67.11	0.99994	311	66.53	0.99996	302	66.82
θ_2		52.97	0.99995	230	70.95	0.99996	209	—
ADSA-P		67.01 ± 0.23						

purposes of the present paper, we therefore do not pursue further the goal of a completely free-standing APF routine. Rather, the fact is used that the routine of inspecting digitized drop profiles like those in Figs. 3 and 4 leads to the choice of the APF contact angle which agrees best with the ADSA-P value. In other words, the four contact angles are compared with the ADSA value and the one giving the best agreement is chosen. It must be realized that this does not make the use of APF redundant, since it does something very different from ADSA-P: APF puts tangents to the drop profile, whereas ADSA fits the best Laplacian shape to the entire profile of the drop. Given the fact that real solid surfaces show typically minor irregularities, leading to minor deviations of the three-phase line from the circular shape, ADSA will average to some extent over such imperfections near the meridian section being imaged. In other words, ADSA, unlike APF, does not give a strictly

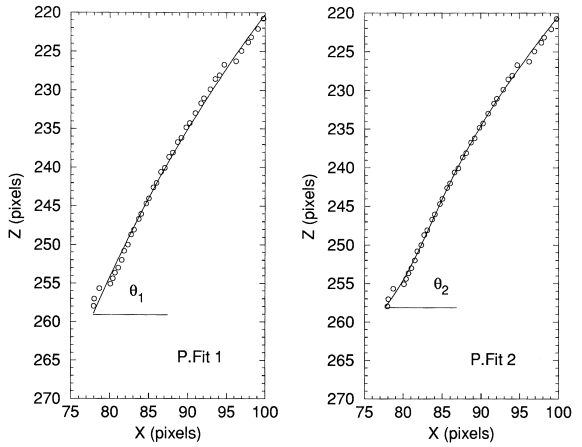

Fig. 3. Close view of the profile coordinates of the drop in Fig. 2 near the left-hand-side contact point, and the best polynomial fits obtained by using the polynomial forms (1) and (2). It can be seen that, in this case, the polynomial fit (2) presents an unreal inflection point owing to the noisy last few coordinate points.

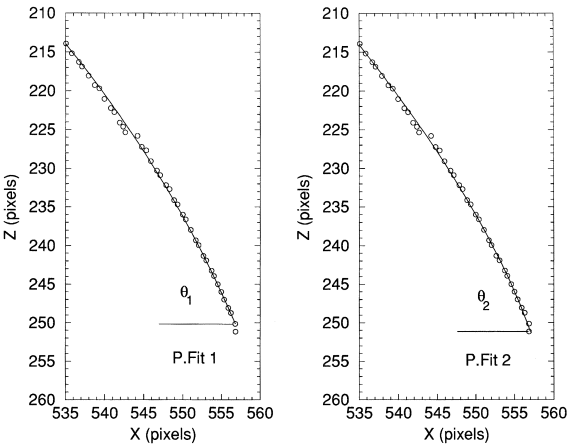

Fig. 4. Close view of the profile coordinates of the drop in Fig. 2 near the right-hand-side contact point, and the best polynomial fits obtained by using the polynomial forms (1) and (2). It can be seen that, in this case, a noisy last coordinate point affects significantly the contact angle obtained with the polynomial fit (2).

two-dimensional account of the meridian section but reflects, to some degree, properties of the solid surface away from this section. Thus, on real solid surfaces, we can expect less scatter in the ADSA data than the APF data. It is hoped that, in the long run, differences between the two kinds of measurement will provide information about the quality of the solid surfaces. Returning to Table 2, we would infer that the APF contact angle is 67.11° and the ADSA-P value is 67.01 ± 0.23.

3. Materials (solid surfaces and liquids)

Two well-prepared solid surfaces were used in this low-rate dynamic contact angle study: a FC-722-coated wafer surface and a poly(propene-*alt*-*N*-methylmaleimide) copolymer-coated surface. Silicon wafers ⟨100⟩ (Silicon Sense, Naschua, NH) were selected as the substrate for contact angle measurements. They were obtained as circular discs of about 10 cm diameter and were cut into rectangular shapes of about 2.5 cm × 5 cm. Each rectangular wafer surface was then soaked in chromic acid for at least 24 h, rinsed with doubly distilled water, and dried under a heat lamp before applying the polymer coating.

FC-722, a 3M "Fluorad" brand fluorochemical coating, available as a 2% solution, was used as supplied. The FC-722-coated surfaces were prepared by a dip-coating technique [5,8] on cleaned and dried silicon wafer surfaces.

Poly(propene-*alt*-*N*-methylmaleimide) copolymer was synthesized by polymer analogous reactions of alternating poly(propene–maleic anhydride) copolymer with methylamine [9]. The chemical structure of the poly(propene-*alt*-*N*-methylmaleimide) copolymer has been described before (for $m=0$ in [1]). The copolymer-coated wafer surfaces were prepared by a solvent-casting technique [1]. A 2% solution was used; it was prepared by using tetrahydrofuran (Sigma-Aldrich, 99+% HPLC) as the solvent. A few drops of the 2% poly(propene-*alt*-*N*-methylmaleimide)/tetrahydrofuran solution were deposited on cleaned silicon wafers inside glass dishes; the solution spread and a thin layer of the copolymer formed on the wafer surface after tetrahydrofuran evaporated overnight. This preparation produced good-quality coated surfaces, as manifested by light fringes owing to refraction at these surfaces, suggesting that the roughness was of the order of nanometres or less.

To perform low-rate dynamic contact angle measurements, liquid was supplied to the sessile drop from below the wafer surfaces with a motorized syringe mechanism [5]. To facilitate such an experimental procedure, a hole of about 1 mm diameter was made, with a diamond drill bit (SMS-0.027) from Lunzer, NY, in the centre of each rectangular wafer surface before soaking in chromic acid. This strategy was pioneered by Oliver et al. [10,11] to measure sessile drop contact angles because of its potential for avoiding drop vibrations and for measuring true advancing contact angles without disturbing the drop profile. In order to avoid leakage between the needle and the hole (on the wafer surface), Teflon tape was wrapped around the end of the needle before inserting it into the hole.

Ten liquids were chosen in this study. Selection of these liquids was based on the following criteria: (1) liquids should include a wide range of intermolecular forces; (2) liquids should be non-toxic; and (3) the liquid surface tension should be higher than the anticipated solid surface tension [12–14]. They are, in the order of increasing surface tension: hexane, 2-octanol, hexadecane, ethanolamine, 1,1,2,2-tetrabromoethane, diiodomethane, 2,2′-thiodiethanol, formamide, glycerol and water. The physical properties and surface tensions of these liquids are shown in Table 3. In order to obtain more accurate results, the liquid surface tensions in Table 3 were obtained by pendant drop experiments using ADSA-P: it has been found that, since ADSA assumes an axisymmetric drop shape, the values of liquid surface tensions measured from sessile drops are very sensitive to even a very small amount of surface imperfection, such as roughness and heterogeneity, while contact angles are less sensitive.

4. Experimental procedures

Details of the experimental procedures for low-rate dynamic contact angles have been described

Table 3
Density, purity and surface tension of the liquids used

Liquid	Supplier	% purity	Density (g cm^{-3})	Surface tension, γ_{lv} (mJ m^{-2})	No. of drops
Hexane	Aldrich	99+	0.659	18.50±0.02	10
2-Octanol	Aldrich	98	0.819	26.00±0.01	9
Hexadecane	Aldrich	99+	0.773	27.62±0.005	10
Ethanolamine	Aldrich	99+	1.012	48.23±0.06	10
1,1,2,2-Tetrabromoethane	Aldrich	98	2.967	49.29±0.05	10
Diiodomethane	Aldrich	99	3.325	49.98±0.02	10
2,2′-Thiodiethanol	Aldrich	99+	1.221	53.77±0.03	10
Formamide	Aldrich	99.5	1.134	59.08±0.01	10
Glycerol	Baker analyzed	99.8	1.258	65.02±0.04	8
Water	LAST[a]	Doubly distilled	0.997	72.70±0.09	10

[a]Laboratory of Applied Surface Thermodynamics.

elsewhere [1,5]. In this study, at least three and up to seven dynamic contact angle measurements at velocities of the three-phase contact line in the range from 0.1 to 0.9 mm min^{-1} were performed for each liquid. The choice of this velocity range was based on previous studies [1,5,15,16] which showed that low-rate dynamic contact angles at these velocities are essentially identical to the static contact angles, at least for these relatively smooth surfaces.

5. Results and discussion

5.1. FC-722-coated surface

Fig. 5(a) shows a typical example of a low-rate dynamic contact angle experiment of glycerol on an inert FC-722-coated surface. The entire experiment was recorded in a sequence of pictures and then analyzed separately by ADSA-P and by the automated polynomial fit program. It can be seen that the ADSA-P contact angles (open symbols) are essentially constant as drop volume increases; further increase in the drop volume causes the three-phase contact line to move. It should be noted that the liquid–vapour surface tension values, γ_{lv}, calculated by ADSA-P are fairly constant, but not as reliable as those from pendant drops, as explained above. The rate of advance for this experiment and other liquids can be determined by linear regression from the linear region of the plot of the three-phase contact radius, R, over time: it was found that the drop periphery was being advanced at a rate of 0.25 mm min^{-1} in the specific example given in Fig. 5(a). Averaging the measured contact angles, after R reaches 0.35 cm, yields a mean contact angle from ADSA-P of 112.07±0.08°, as discussed before [1].

The contact angle results calculated by the APF program are also given in Fig. 5(a) in solid symbols. It can be seen that the APF contact angles are essentially the same as those from ADSA-P, but with more scatter. Presumably, this is due to minute surface heterogeneity and/or roughness of the surface which cause noisy coordinates near the three-phase contact points, as discussed in connection with Figs. 3 and 4. The averaged APF contact angle is found to be 113.64±1.35°; i.e., a value in good agreement with that from ADSA-P. A total of five experiments at different rates of advance was performed for glycerol, each on a newly prepared surface. The results for both techniques are summarized in Table 4, together with the results for other liquids. Since the contact angles of glycerol at different rates of advance (in Table 4) are essentially constant, they can be averaged and result in a final ADSA-P contact angle of 111.89±0.30° and a final APF contact angle of 112.72±1.26°. This result illustrates the good agreement between the two techniques.

Fig. 5(b)–(d) show similar low-rate dynamic contact angle results for hexadecane, 2-octanol, and hexane, respectively. A total of seven experiments for hexadecane and three experiments for 2-octanol and hexane were performed on a new

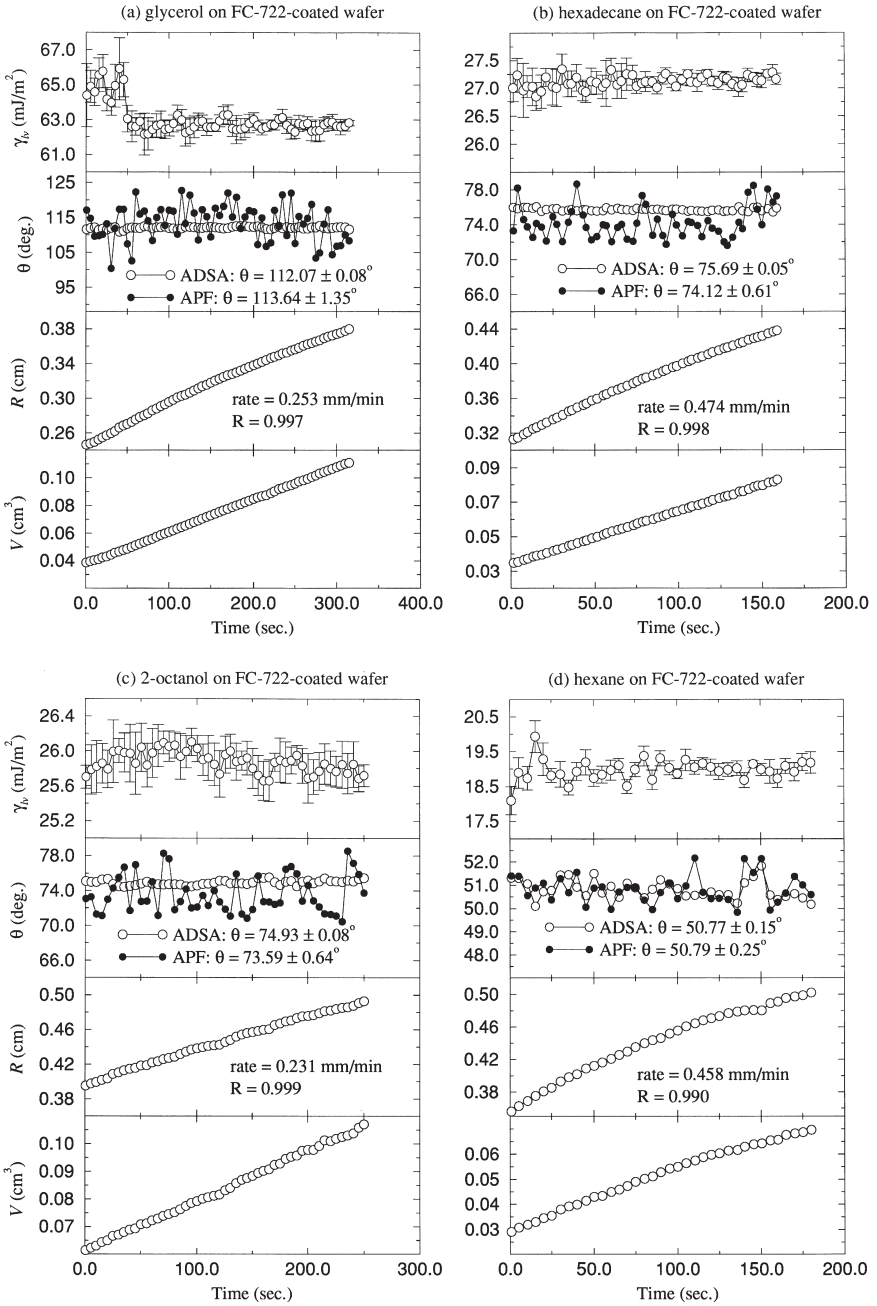

Fig. 5. Low-rate dynamic contact angles of (a) glycerol, (b) hexadecane, (c) 2-octanol and (d) hexane, on FC-722-coated wafer surface measured by ADSA-P and the APF program; γ_{lv}, θ, R and V are, respectively, the liquid–vapour surface tension, contact angle, three-phase contact radius, and drop volume; R is the regression coefficient. Good agreement was found between the two techniques.

Table 4
Low-rate dynamic contact angles (degrees) measured by ADSA-P and the APF program on a FC-722-coated silicon wafer surface. The rate of advancing of the three-phase contact line is in mm min^{-1}. The error bars are 95% confidence limits

Glycerol			Hexadecane			2-Octanol			Hexane		
Rate	θ (ADSA-P)	θ (APF)	Rate	θ (ADSA-P)	θ (APF)	Rate	θ (ADSA-P)	θ (APF)	Rate	θ (ADS-P)	θ (APF)
0.253	112.07 ± 0.08	113.64 ± 1.35	0.185	75.73 ± 0.08	73.50 ± 0.69	0.231	74.93 ± 0.08	73.59 ± 0.64	0.431	50.89 ± 0.14	51.40 ± 0,39
0.281	111.67 ± 0.15	112.87 ± 1.07	0.194	75.67 ± 0.04	73.77 ± 0.39	0.345	74.70 ± 0.07	73.65 ± 0.55	0.458	50.77 ± 0.10	50.79 ± 0.25
0.412	111.67 ± 0.12	111.81 ± 1.54	0.207	75.72 ± 0.04	74.25 ± 0.66	0.681	74.60 ± 0.07	73.04 ± 0.74	0.510	50.82 ± 0.12	51.20 ± 0.27
0.599	111.84 ± 0.16	111.54 ± 2.76	0.239	75.59 ± 0.02	73.28 ± 0.31	—	—	—	—	—	—
0.828	112.20 ± 0.18	113.72 ± 2.40	0.474	75.69 ± 0.05	74.12 ± 0.61	—	—	—	—	—	—
—	—	—	0.478	75.48 ± 0.07	73.14 ± 0.51	—	—	—	—	—	—
—	—	—	0.497	75.60 ± 0.07	73.76 ± 0.46	—	—	—	—	—	—
Mean θ	111.89 ± 0.30	112.72 ± 1.26		75.64 ± 0.08	73.69 ± 0.38		74.74 ± 0.42	73.43 ± 0.84		50.83 ± 0.15	51.16 ± 0.87

Table 5
Summary of contact angles measured by ADSA-P and the APF program on a FC-722-coated silicon wafer surface

Liquid	Surface tension (mJ m^{-2})	Contact angle (degrees)	
		ADSA-P	APF
Hexane	18.50	50.83 ± 0.15	51.16 ± 0.87
2-Octanol	26.00	74.74 ± 0.42	74.43 ± 0.84
Hexadecane	27.62	75.64 ± 0.08	73.69 ± 0.38
Glycerol	65.02	111.89 ± 0.30	112.72 ± 1.26

solid surface each time. The results are summarized in Table 4. It can be seen, in general, that the APF contact angles have larger scatter than those from ADSA-P.

It should be noted that, in Fig. 5(a)–(c), the APF contact angles tend to have larger scatter than those from ADSA-P, while in Fig. 5(d), the APF contact angles essentially overlap with those from ADSA-P. Such results are not surprising, and are due to the fact that the drop profiles in Fig. 5(a)–(c) have more noisy data near the contact points, causing more scatter in the APF contact angles. Therefore, use of both ADSA-P and the APF scheme for measuring contact angles may provide additional information on the quality of the experiments. A summary of the contact angles calculated by ADSA-P and APF is shown in Table 5.

5.2. *Poly(propene-alt-N-methylmaleimide)*

Fig. 6(a) shows an example of a low-rate dynamic contact angle experiment of water on a poly(propene-*alt*-*N*-methylmaleimide) copolymer surface. As can be seen in the ADSA-P results (open symbols), increasing the drop volume, V, linearly from about 0.06 cm^3 to 0.07 cm^3 increases the apparent contact angle, θ, from about 65° to 70° at essentially constant contact radius. This increase in the contact angle has been explained before [1] and is due to the fact that even carefully putting an initial water drop from above on a solid surface can result in a contact angle somewhere between advancing and receding. This effect is more pronounced for liquids, such as water, which evaporate fast. Thus, it takes time for the initial drop front to start advancing. Further increase in the drop volume causes the three-phase contact line to advance, with θ essentially constant as R increases. Averaging the measured contact angles yields a mean ADSA-P contact angle of $70.19 \pm 0.10°$. The contact angle results calculated by the automated polynomial fit (APF) program are also given in solid symbols. Again, the APF contact angles are essentially the same as those from ADSA-P, but with more scatter. A mean APF contact angle of $69.14 \pm 0.27°$ is obtained, in good agreement with that from ADSA-P. A summary of all experimental results for this and other liquids is shown in Table 6. In the case of glycerol, the experimental contact angles (not shown) were found to be very constant, similar to those shown in Fig. 6(a). Six experiments (for six different rates of advance) were performed in total on a new solid surface each time, as given in Table 6.

In Fig. 6(b), a contact angle experiment of formamide is shown. It can be seen from the ADSA-P results that, as the drop volume increases initially, the contact angle increases from about 40° to 42° and the surface tension decreases from about 58 mJ m^{-2} to 54 mJ m^{-2}. As drop volume continues to increase, the contact angle decreases from about 42° to 39°. These contact angle patterns have been observed in a previous paper [1]: it is apparent that dissolution of the copolymer occurs, causing the liquid–vapour surface tension to change from that of the pure liquid. It should be noted that a general trend of such contact angle patterns was also observed by the APF program, but with larger scatter. Since chemical or physical reactions such as polymer dissolution change the liquid–vapour, solid–vapour and solid–liquid interfaces (interfacial tensions) in an unknown manner and since we are unsure whether or not

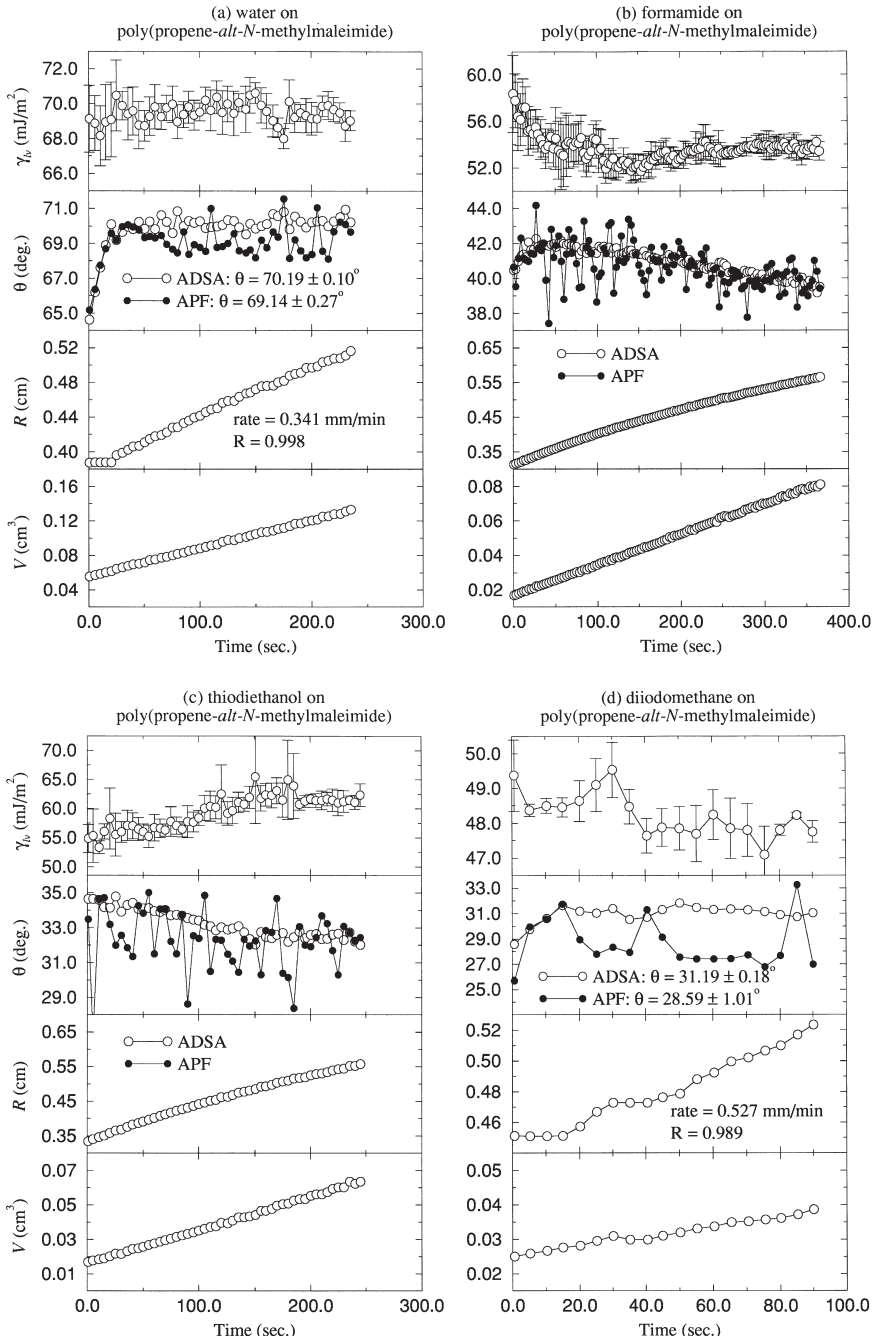

Fig. 6. Low-rate dynamic contact angles of (a) water, (b) formamide, (c) 2,2′-thiodiethanol and (d) diiodomethane, on a poly(propene-*alt*-*N*-methylmaleimide) copolymer measured by ADSA-P and APF. γ_{lv}, θ, R and V are, respectively, the liquid–vapour surface tension, contact angle, three-phase contact radius, and drop volume; R is the regression coefficient. Good agreement was found between the two techniques. The decrease in both the liquid–vapour surface tension and the contact angle in (b) and (c) suggest dissolution of the copolymer. A decreasing trend of the contact angles was also observed by the APF scheme, with larger scatter. These contact angles are disregarded for the interpretation in terms of surface energetics.

Table 6
Low-rate dynamic contact angles, θ (degrees), measured by ADSA-P and the APF program on a poly(propene-*alt*-*N*-methylmaleimide) copolymer. The rate of advancing of the three-phase contact line is in mm min^{-1}. The error bars are 95% confidence limits

Water			Glycerol			Diiodomethane		
Rate	θ (ADSA-P)	θ (APF)	Rate	θ (ADSA-P)	θ (APF)	Rate	θ (ADSA-P)	θ (APF)
0.146	69.22±0.04	68.56±0.12	0.219	60.73±0.04	60.56±0.14	0.480	29.78±0.14	30.99±1.31
0.158	70.23±0.07	69.22±0.15	0.253	59.67±0.06	59.58±0.30	0.527	31.19±0.18	28.59±1.01
0.183	69.69±0.06	68.84±0.15	0.256	60.28±0.04	60.30±0.20	0.669	30.43±0.19	28.05±2.69
0.208	69.95±0.06	69.67±0.16	0.297	60.11±0.06	59.96±0.20	0.789	31.48±0.20	28.04±0.79
0.314	69.56±0.10	69.48±0.21	0.409	60.44±0.10	60.64±0.23	0.813	30.69±0.35	25.49±2.91
0.341	70.19±0.10	69.14±0.27	0.527	60.25±0.08	60.54±0.31	—	—	—
Mean θ	69.81±0.41	69.15±0.43		60.25±0.37	60.26±0.44		30.71±0.83	28.23±2.43

the solid–vapour surface tension, γ_{sv}, will remain constant and whether Young's equation is applicable, the contact angle data in Fig. 6(b) should be disregarded for the interpretation in terms of surface energetics: all contact angle approaches [12,13,17–20] assume the constancy of γ_{lv}, γ_{sv} and γ_{sl} and the validity of Young's equation.

Fig. 6(c) shows the contact angle results of 2,2′-thiodiethanol: as drop volume increases continuously, the ADSA-P contact angle decreases from about 35° to 32°, with a slight increase in the apparent surface tension value. The decreasing trend of the contact angles is also observed by APF, in spite of larger scatter. Indeed, it was observed after the experiment that the copolymer layer in the area of contact between 2,2′-thiodiethanol and the copolymer appeared to be partly removed. These contact angles are disregarded in terms of the interpretation of surface energetics.

Fig. 6(d) shows the contact angle results of diiodomethane. The ADSA-P contact angles are essentially constant after the initial pick-up and hence the essentially constant angles are averaged. The averaged ADSA-P contact angle is found to be 31.19±0.18° at a rate of advance of 0.53 mm min^{-1}. It should be noted that the APF contact angles show larger variation. The averaged APF contact angle yields 28.59±1.01°. A total of five experiments was performed and the results are shown in Table 6.

It was found that ethanolamine and 1,1,2,2-tetrabromoethane dissolved the copolymer on contact. Table 7 summarizes and compares the contact angles obtained by ADSA-P and APF for water, glycerol, formamide, 2,2′-thiodiethanol and diiodomethane. Since physiochemical reactions take place for formamide and 2,2′-thiodiethanol, these contact angles are rejected for the interpretation in terms of surface energetics.

It is interesting to note in Tables 5 and 7 that,

Table 7
Summary of contact angles measured by ADSA-P and the APF program on a poly(propene-*alt*-*N*-methylmaleimide) copolymer

Liquid	Surface tension (mJ m^{-2})	Contact angle (degrees)	
		ADSA-P	APF
Ethanolamine	48.23	Dissolved the polymer on contact	
1,1,2,2-Tetrabromoethane	49.29	Dissolved the polymer on contact	
Diiodomethane	49.98	30.71±0.83	28.23±2.43
2,2′-Thiodiethanol	53.77	$\theta\downarrow$ and $\gamma_{lv}\uparrow$ as $R\uparrow$ (36°→32°)	$\theta\downarrow$ as $R\uparrow$
Formamide	59.08	$\theta\downarrow$ and $\gamma_{lv}\downarrow$ as $R\uparrow$ (44°→41°)	$\theta\downarrow$ as $R\uparrow$
Glycerol	65.02	60.25±0.37	60.26±0.44
Water	72.80	69.81±0.41	69.15±0.43

for $\theta<90^\circ$, the APF contact angles (of 2-octanol, hexadecane, diiodomethane and water) are consistently smaller than those from ADSA-P, while for $\theta>90^\circ$, the APF contact angle (of glycerol) is larger than that of ADSA-P. This result is in agreement with the expectation that minute surface heterogeneity and/or roughness of some of the surfaces are indeed present. For $\theta<90^\circ$, surface roughness and/or heterogeneity would make the three-phase contact line creep locally and since the APF scheme reflects heavily coordinates near the contact points, the resulting APF contact angle is expected to be smaller than it should be. For $\theta>90^\circ$, on the other hand, such an effect would pinch the drop along the three-phase contact line, causing a APF contact angle larger than expected on a more perfect solid. Thus, use of both ADSA-P and APF schemes may provide additional information on the quality of the surface. In the case of hexane/FC-722 in Table 5 and glycerol/poly (propene-*alt*-*N*-methylmaleimide) in Table 7, the excellent agreement between the two techniques probably illustrates the good surface quality and the inert character of the solid surface.

If the inconclusive contact angles of formamide and 2,2′-thiodiethanol on the non-inert poly(propene-*alt*-*N*-methylmaleimide) copolymer are omitted, smooth curves emerge when plotting the values of $\gamma_{lv}\cos\theta$ against γ_{lv}. Fig. 7 shows this plot using the mean contact angles from ADSA-P and the APF scheme (in Tables 5 and 7) as well as contact angles from other studies [1,5,8,15,21]. It can be seen in this figure that the values of $\gamma_{lv}\cos\theta$ all change smoothly with γ_{lv} for the inert (non-polar) FC-722-coated surface and for the non-inert (polar) poly(propene-*alt*-*N*-methylmaleimide) copolymer, regardless of intermolecular forces. When comparing with the previous maleimide copolymer surfaces, a coherent change in the wettability is observed as the length of the side chains decreases from hexyl to methyl groups. These patterns are also in excellent agreement with our previous results for other polymer surfaces [8,22–24]. Clearly, contact angle patterns different from

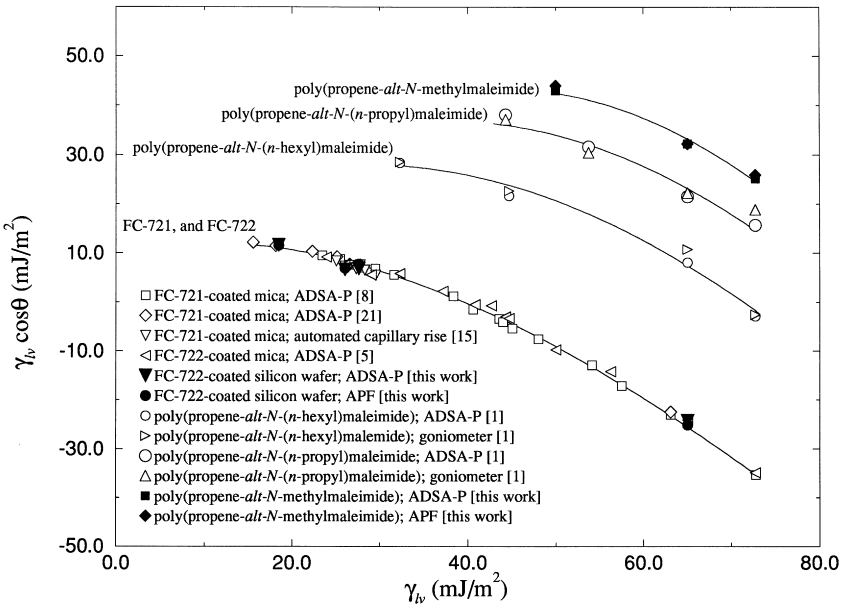

Fig. 7. The values of $\gamma_{lv}\cos\theta$ vs. γ_{lv} for FC-721-coated mica [8,15,21], FC-722-coated mica [5] and silicon wafer [this work], Teflon (FEP) [8,15], poly(propene-*alt*-*N*-(n-hexyl)maleimide) [1], poly(propene-*alt*-*N*-(n-propyl)maleimide) [1] and poly(propene-*alt*-*N*-methylmaleimide) [this work]. Excluding the inconclusive contact angle data for poly(propene-*alt*-*N*-methylmaleimide), the values of $\gamma_{lv}\cos\theta$ all change smoothly with γ_{lv}, independent of which of the experimental methods is used. A systematic change in the wettability can be observed as the length of the side chains for the maleimide copolymer decreases from hexyl to methyl groups.

those in Fig. 7 are due to bad experimentation, poor surface quality, and/or lack of inertness of the solid surface.

6. Conclusions

(1) There is broad agreement between ADSA-P and APF contact angle results.
(2) Small deviations between the two approaches may be caused by imperfections of the solid surface.
(3) Producing a good APF scheme is a task far from trivial, and available schemes should be used with circumspection.
(4) Circumspection is necessary in the decision whether or not experimental contact angles can be used in conjunction with Young's equation, as stated before [1].

Acknowledgment

This research was supported by the Natural Science and Engineering Research Council of Canada (Grant Nos A8278 and EQP173469), a Ontario Graduate Scholarship (D.Y.K.), and a University of Toronto Open Fellowship (D.Y.K.).

References

[1] D.Y. Kwok, T. Gietzelt, K. Grundke, H.-J. Jacobasch, A.W. Neumann, Langmuir 13 (1997) 2880.
[2] Y. Rotenberg, L. Boruvka, A.W. Neumann, J. Colloid Interface Sci. 93 (1983) 169.
[3] P. Cheng, D. Li, L. Boruvka, Y. Rotenberg, A.W. Neumann, Colloids Surfaces 93 (1983) 169.
[4] S. Lahooti, O.I. del Río, P. Cheng, A.W. Neumann, in: A.W. Neumann, J.K. Spelt (Eds.), Applied Surface Thermodynamics, Marcel Dekker, New York, 1996, pp. 441–507.
[5] D.Y. Kwok, R. Lin, M. Mui, A.W. Neumann, Colloids Surfaces A: Physicochem. Eng. Aspects 116 (1996) 63.
[6] O.I. del Río, A.W. Neumann, J. Colloid Interface Sci., accepted for publication.
[7] D. Li, A.W. Neumann, in: A.W. Neumann, J.K. Spelt (Eds.), Applied Surface Thermodynamics, Marcel Dekker, New York, 1996, pp. 109–168.
[8] D. Li, A.W. Neumann, J. Colloid Interface Sci. 148 (1992) 190.
[9] U. Wienhold, PhD Thesis, Martin-Luther-Universität Halle-Wittenberg, Germany, 1994.
[10] J.F. Oliver, C. Huh, S.G. Mason, J. Colloid Interface Sci. 3 (1977) 568.
[11] J.F. Oliver, C. Huh, S.G. Mason, Colloids Surfaces A: Physicochem. Eng. Aspects 1 (1980) 79.
[12] W.A. Zisman, in: Advances in Chemistry Series, vol. 43, American Chemical Society, Washington, D.C., 1964.
[13] J.K. Spelt, D. Li, in: A.W. Neumann, J.K. Spelt (Eds.), Applied Surface Thermodynamics, Marcel Dekker, New York, 1996, pp. 239–292.
[14] K. Grundke, T. Bogumil, T. Gietzelt, H.-J. Jacobasch, D.Y. Kwok, A.W. Neumann, Prog. Colloid Polym. Sci. 101 (1996) 58.
[15] D.Y. Kwok, C.J. Budziak, A.W. Neumann, J. Colloid Interface Sci. 173 (1995) 143.
[16] D.Y. Kwok, D. Li, A.W. Neumann, in: A.W. Neumann, J.K. Spelt (Eds.), Applied Surface Thermodynamics, Marcel Dekker, New York, 1996, pp. 413–440.
[17] A.W. Neumann, R.J. Good, C.J. Hope, M. Sejpal, J. Colloid Interface Sci. 49 (1974) 291.
[18] F.M. Fowkes, Ind. Eng. Chem. 12 (1964) 40.
[19] C.J. van Oss, M.K. Chaudhury, R.J. Good, Chem. Rev. 88 (1988) 927.
[20] R.J. Good, C.J. van Oss, in: M. Schrader, G. Loeb. (Eds.), Modern Approaches to Wettability: Theory and Applications, Plenum Press, New York, 1992, pp. 1–27.
[21] D. Li, M. Xie, A.W. Neumann, Colloid Polym. Sci. 271 (1993) 573.
[22] G.H.E. Hellwig, A.W. Neumann, in: Proceedings of the Fifth International Congress on Surface Activity, Section B, Barcelona, 1968, p. 687.
[23] G.H.E. Hellwig, A.W. Neumann, Kolloid Z. Z. Polym. 40 (1969) 229.
[24] D.Y. Kwok, D. Li, A.W. Neumann, Colloids Surfaces A: Physicochem. Eng. Aspects. 89 (1994) 181.